Contents lists available at ScienceDirect

Medical Engineering and Physics

journal homepage: www.elsevier.com/locate/medengphy

Paper

Predicting the effects of surgically determined parameters on exercise tolerance in Fontan patients

Poom Kritpracha [a,c], Beatrice Riviere [a], Charles Puelz [b,*]

[a] Department of Computational Applied Mathematics and Operations Research, Rice University, Houston, TX, USA
[b] Department of Pediatrics, Division of Cardiology, Baylor College of Medicine and Texas Children's Hospital, Houston, TX, USA
[c] Department of Applied Mathematics, University of Colorado Boulder, Boulder, CO, USA

A B S T R A C T

The Fontan physiology is a surgically created circulation for patients with a single functioning ventricle. Patients with this circulation tend to have lower exercise tolerance compared to those with a normal circulation. Important computational and experimental work has been done to investigate this reduction in exercise tolerance. However, there are few systematic modeling studies that focus on the effect of several surgically determined parameters within the same framework. We propose a mathematical model to describe the Fontan circulation under exercise. We then formulate a heuristic based on clinical data from Fontan patients to estimate exercise tolerance. The model is used to investigate the effect of three important surgically determined parameters on exercise tolerance: the systemic arterial compliance, the systemic-venous to pulmonary-venous fenestration, and the resistance of the total cavopulmonary connection.

1. Introduction

The Fontan procedure is a common operation for patients with single ventricle physiology [14]. It is usually the third intervention in a sequence of operations that gradually establish a serial circulation with a single ventricle pump. For patients with hypoplastic left heart syndrome, the circulation is created by reconstructing and connecting the aorta to the right ventricle and connecting the vena cavae to the pulmonary arteries. The surgical reconstruction of the aorta impacts the systemic arterial compliance, partially due to the patch material used in building the new vessel needed for ventricular outflow [2,27]. The connection of the vena cavae and pulmonary arteries, referred to as the total cavopulmonary connection (TCPC), places the systemic organs and lungs in series and establishes passive pulmonary blood flow. Fontan patients generally have lower cardiac output and higher pulmonary arterial pressure in part due to their abnormal physiology and passive flow to the lungs. To mitigate these issues, an additional surgical connection between the systemic and pulmonary veins, called a fenestration, is optionally introduced. In this paper, we develop a computer model of the Fontan circulation to study the impact of these three surgically determined parameters, i.e. the systemic arterial compliance, TCPC resistance, and fenestration size, on exercise tolerance.

The invention of the Fontan procedure marked a significant advance in the treatment of congenital heart disease [14,29,13]. However, Fontan patients have limited exercise tolerance [15,4,20,24]. Furthermore, the study of exercise tolerance in Fontan patients is of critical importance; it has been observed that a decrease in exercise tolerance is a predictor of subsequent hospitalization and death [43,12]. While there is some clinical research evaluating this reduction in exercise tolerance as well as studying how surgical decisions may impact it, investigations from a computer modeling perspective remain relatively scarce [11]. Of note is the work from Kung et al., who created a compartmental Fontan model with exercise predictions that were consistent with clinical data [21]. Their approach was used to predict the effects of several types of cardiac dysfunction on exercise tolerance [22]. Marsden et al. created a 3D modeling framework to simulate local fluid mechanics within the TCPC [28]. The authors studied TCPC fluid flow at rest and at different levels of exercise. Our paper complements these previous works by developing a compartmental Fontan model to systematically examine the impact of several important surgical decisions on exercise tolerance. To our knowledge, the effects of the systemic arterial compliance, TCPC resistance, and fenestration size on exercise tolerance have not been studied in the same computer modeling framework.

The work presented in this paper builds upon the at-rest fenestrated Fontan model from Ahmad et al. [1]. We extend this model to encompass the Fontan physiology under exercise. Specifically, section 2 discusses the at-rest compartmental model and its calibration to clinical data. Then, we discuss an empirically motivated model that describes

* Corresponding author.
E-mail address: charles.puelz@bcm.edu (C. Puelz).

https://doi.org/10.1016/j.medengphy.2024.104152
Received 18 May 2023; Received in revised form 15 February 2024; Accepted 11 March 2024

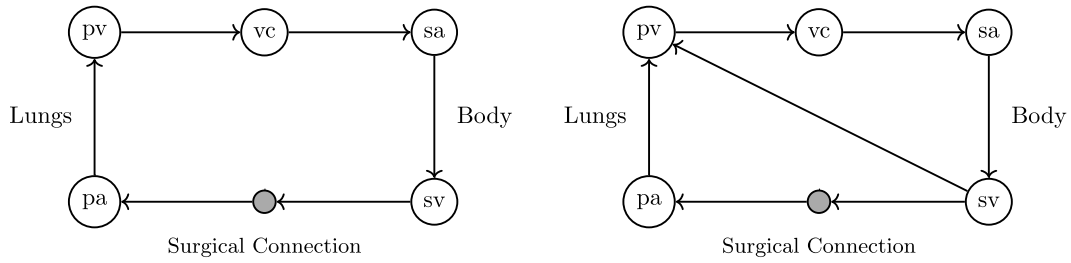

(a) without fenestration. (b) with fenestration.

Fig. 1. Compartmental model for the Fontan physiology.

physiological adaptations to exercise, and we provide a heuristic to estimate exercise tolerance from the model predictions. Section 3 details the results, including a comparison of the exercise model to clinical data. Finally, we use the model to predict how the systemic arterial compliance, TCPC resistance, and fenestration size affect exercise tolerance.

2. Methods

2.1. At-rest model and calibration

In this paper, the Fontan circulation is modeled by five compartments: the ventricular chamber (vc), the systemic arteries (sa), the systemic veins (sv), the pulmonary arteries (pa) and the pulmonary veins (pv); refer to Fig. 1a. A surgical connection called the total cavopulmonary connection links the systemic venous and pulmonary arterial compartments, allowing for passive flow from the systemic veins to the lungs in the absence of a ventricular chamber. The quantities of interest for compartment i are the blood pressure P_i and volumetric concentration of oxygen σ_i. The volumetric concentration of oxygen is related to the oxygen saturation Sat_i in compartment i by the equation $\sigma_i = 0.201 \times \mathrm{Sat}_i/100$. This relationship ensures that $\mathrm{Sat}_i = 100\%$ corresponds to $\sigma_i = 0.201$, the maximum volumetric concentration of oxygen in blood [8,33].

Ahmad et al. [1] demonstrated that this compartmental model can be used to effectively describe the Fontan circulation with and without a fenestration. Each compartment i is described by a compliance C_i and a volume V_i. The time-dependent compliance for the ventricular chamber depends on the end-systolic compliance C_{sys} and the end-diastolic compliance C_{dias}, and it is defined by the following equations:

$$C_{\mathrm{vc}}(t) = \left(\left(\frac{1}{C_{\mathrm{sys}}} - \frac{1}{C_{\mathrm{dias}}} \right) \frac{\psi(t)}{\|\psi\|_\infty} + \frac{1}{C_{\mathrm{dias}}} \right)^{-1}, \tag{1}$$

$$\psi(t) = \frac{g_1(t)}{1+g_1(t)} \left(\frac{1}{1+g_2(t)} - \frac{1}{1+g_2(T)} \right), \quad g_i(t) = \left(\frac{t}{\tau_i} \right)^{m_i}. \tag{2}$$

Paths between two compartments are described by resistances: R_{av} for the path $(\mathrm{pv}, \mathrm{vc})$, R_{ao} for the path $(\mathrm{vc}, \mathrm{sa})$, R_{s} for the path $(\mathrm{sa}, \mathrm{sv})$, R_{TCPC} for the path $(\mathrm{sv}, \mathrm{pa})$, and R_{p} for the path $(\mathrm{pa}, \mathrm{pv})$. Mass balance equations written for each compartment lead to a nonlinear system of ordinary differential equations for the pressures P_i and the concentrations σ_i. Details are provided in appendix A.1.

2.2. Surgical fenestration

The fenestration is an additional connection that is optionally placed within the Fontan circulation, depending on physiological conditions. The main benefits of such a connection are a decrease in pulmonary artery pressure and an increase in cardiac output. Fig. 1b shows the compartmental model with the fenestration represented by the segment between compartments sv and pv. The fenestration resistance is denoted by R_{fen}. The size of the fenestration is incorporated into the model using the Gorlin equation. The resistance is determined by the fenestration cross-sectional area A_{fen} and the pressure gradient through the connection (sv,pv) via the following relationship [1,17]:

$$R_{\mathrm{fen}} = R_0 + \frac{\rho}{2R_{\mathrm{fen}}A_{\mathrm{fen}}^2} |P_{\mathrm{sv}} - P_{\mathrm{pv}}|. \tag{3}$$

The parameters ρ and R_0 are the density of blood and the viscous resistance of the fenestration when flow is close to zero, respectively:

$$\rho = 1.06 \text{ g ml}^{-1} = 2.2085 \times 10^{-5} \text{ mmHg min}^2 \text{ dm}^{-2},$$

$$R_0 = 10^{-3} \text{ mmHg min L}^{-1}.$$

We note that the resistance R_{fen} depends nonlinearly on the pressures in the sv and pv compartments. Furthermore, equation (3) can be rewritten as a quadratic root finding problem for $R_{\mathrm{fen}} > 0$,

$$R_{\mathrm{fen}}^2 - R_0 R_{\mathrm{fen}} - \frac{\rho}{2A_{\mathrm{fen}}^2} |P_{\mathrm{sv}} - P_{\mathrm{pv}}| = 0, \tag{4}$$

in which the fenestration resistance is the distinct positive root.

2.3. Exercise model

In this work, exercise intensity is quantified through the body's systemic oxygen consumption rate $\dot{V}O_2$. To take into account the physiological adaptations to exercise, we propose models for the heart rate, systemic resistance, systemic arterial compliance, single ventricle compliance, and venous dead volume as functions of the exercise intensity. The relationship between heart rate and oxygen consumption rate is determined from experimental data by Hedlund et al. [19] and is fitted to a linear relation [40]:

$$HR = 71.093 \, \dot{V}O_2 + 60.441 \text{ min}^{-1}. \tag{5}$$

In order to approximate exercise-induced changes in systemic resistance and arterial compliance, we derive relationships based on experimental results from Larsson et al. [23]. Fontan patients in their study underwent exercise, and cardiopulmonary parameters were recorded at both rest and maximal exercise. While the work from Larsson et al. [23] does not include measurements of arterial compliance C_{sa}, it contains measurements of stroke volume SV, systolic blood pressure SBP, and diastolic blood pressure DBP, which we can use to approximate compliance by the following relation (see [31]):

$$C_{\mathrm{sa}} \approx \frac{SV}{SBP - DBP}. \tag{6}$$

Furthermore, we assume that exercise-induced parameter changes can be described as an power law function of heart rate. For a physiological parameter x with an at-rest value of x_0, power law exponent γ, and resting heart rate HR_0, the exercise-induced change in the parameter is expressed as

$$x = x_0 \left(\frac{HR_0}{HR} \right)^\gamma, \tag{7}$$

where x_0 is the at-rest value of the parameter specified in appendix A.2. We used tabulated data collected at rest and at maximal exercise from Larsson et al. to estimate the power law exponent γ for the systemic resistance and arterial compliance [23]. Rounding to two significant digits, we obtain the exponential factors $\gamma = 0.57$ and $\gamma = 0.37$ for R_s and C_{sa} respectively. Therefore, we propose the following relations to describe exercise-induced changes in the systemic compartment:

$$R_s = R_{s,0}\left(\frac{HR_0}{HR}\right)^{0.57} \quad \text{mmHg} \cdot \text{min} \cdot \text{L}^{-1}, \tag{8}$$

$$C_{sa} = C_{sa,0}\left(\frac{HR_0}{HR}\right)^{0.37} \times 10^{-4} \quad \text{L} \cdot \text{mmHg}^{-1}. \tag{9}$$

Following the exercise model from Han et al. [17], we model systemic venous dead volume as a function of heart rate in the following way:

$$V_{d,sv} = V_{d,sv,0}\left(\frac{HR_0}{HR}\right)^{0.1} \quad \text{L}. \tag{10}$$

Finally, the change in ventricular contractility is modeled by varying the end-systolic and end-diastolic compliance of the ventricle chamber. In exercise, the end-systolic compliance decreases and the end-diastolic compliance increases so that stroke volume matches the body's demand for oxygen. A decrease in end-systolic compliance corresponds to stronger ventricular contraction and an increase in end-diastolic compliance allows for adequate ventricular filling. The exercise-induced change in the end-systolic relationship is estimated from Najjar et al. [30] for healthy individuals under the age of 40:

$$C_{sys} = C_{sys,0}\left(\frac{HR_0}{HR}\right)^{1.8} \quad \text{L} \cdot \text{mmHg}. \tag{11}$$

The variation in end-diastolic compliance is chosen such that the resulting cardiac output attains a reasonable range and the predicted exercise tolerance, as described in the coming sections, aligns well with clinical data:

$$C_{dias} = C_{dias,0}\left(\frac{HR_0}{HR}\right)^{-0.2} \quad \text{L} \cdot \text{mmHg}. \tag{12}$$

The at-rest heart rate HR_0 is evaluated from equation (5) with $\dot{V}O_2 = 0.2\ \text{L} \cdot \text{min}^{-1}$. The cycle period is the inverse of the heart rate:

$$T = \frac{1}{HR} \quad \text{min}.$$

2.4. Exercise tolerance estimation

The baseline model in section 2.1 and the exercise adaptations described in section 2.3 give a description of the physiologic response while undergoing exercise at a specific intensity. For a given oxygen consumption rate, the model predicts the physiologic response in terms of time-dependent compartment pressures and oxygen concentrations. Since oxygen is consumed in the tissues between systemic arterial and systemic venous compartments, the systemic venous oxygen concentration σ_{sv} is related to the body's response to the corresponding level of exercise. Qualitatively, a lower σ_{sv} implies worse exercise tolerance as, per Fick's law, the body is not able to adequately match the cardiac output to its oxygen needs. However, since this is only an approximate means for measuring exercise response, we sought to establish a more precise method for quantifying exercise tolerance in the context of this model. Although the characterization of exercise tolerance is generally malleable and depends on the type of exercise, the maximal oxygen consumption rate, $\dot{V}O_2$-max, i.e. the maximal rate at which the body can metabolically utilize oxygen, is a widely used metric for quantifying an individual's exercise tolerance [38].

We propose a heuristic method for estimating $\dot{V}O_2$-max from our compartmental model using the predicted systemic venous oxygen saturation Sat_{sv}. Shachar et al. measured an average venous oxygen saturation of 31% in exercising Fontan patients [37]. Although their data did not include maximal oxygen consumption rate or other metrics for maximal exercise tolerance, we cross-examine their results with those of Hedlund et al. [19] via the patients' work output during exercise. In the work of Shachar et al., the body surface area indexed work rate was estimated to be 40-60 $\text{W} \cdot \text{m}^{-2}$ [37]. For an average body surface area of 1.5 m^2, the absolute work rate was 60-90 W. Taking the oxygen consumption rate at maximal exercise from the work of Hedlund et al. to correspond to 100% of the $\dot{V}O_2$-max, the average work rate from Shachar et al. would correspond to approximately 75% of the $\dot{V}O_2$-max. Thus, for the purposes of our analysis, we assume that $0.75 \cdot \dot{V}O_2$-max is the oxygen consumption that results in a systemic venous saturation of 31%.

Table 1
Hemodynamic variables predicted by the model for the scenarios of at-rest ($\dot{V}O_2 = 0.20\ \text{L} \cdot \text{min}^{-1}$), moderate ($0.885\ \text{L} \cdot \text{min}^{-1}$), and maximal exercise ($1.570\ \text{L} \cdot \text{min}^{-1}$).

Variable	At-rest	Moderate	Maximal
Systolic Blood Pressure (mmHg)	120.03	162.30	182.46
Diastolic Blood Pressure (mmHg)	69.69	92.00	102.09
Cardiac Output ($\text{L} \cdot \text{min}^{-1}$)	4.26	7.67	10.32
Stroke Volume (mL)	57.00	62.17	59.97
Systemic Oxygen Saturation (%)	95	95	95
Venous Oxygen Saturation (%)	70.39	34.56	15.32

2.5. Numerical methods

The system of nonlinear ordinary differential equations is discretized using the backward Euler time-stepping scheme. This approach gives rise to a nonlinear system where the nonlinearity appears in the valve states as well as the resistance of the fenestration in equation (3). We use a fixed-point iterative method to solve the nonlinear system. Iterations are stopped when the residual is sufficiently small. Details of the numerical algorithm are provided in appendix A.3. Initial conditions are as follows: compartmental pressures are set to zero, except for $P_{sv} = 11.6909$ mmHg; this implies that the blood volume is 5 L. Compartmental concentrations in each compliance chamber are set to $0.15\ \text{L}_{O_2}/\text{L}_{\text{blood}}$. Simulations are run for 1000 cardiac cycles with 200 timesteps per cardiac cycle. We found that, for our system and these parameters, solutions obtain a periodic steady state within this number of cycles.

3. Results

3.1. Baseline exercise model

In this section, we verify that our model predicts variables within reasonable ranges compared to available clinical data. A baseline version of the model described in sections 2.1 and 2.3 is tested for the case of a closed fenestration. Parameters values are based on Ahmad et al. [1] except for R_{TCPC}, which is determined based on data that characterizes energy losses in total cavopulmonary connections [41,44,34]. Exercise intensity is characterized by the systemic oxygen consumption $\dot{V}O_2$. In our first set of tests, we simulate three scenarios: at-rest, moderate exercise, and maximal exercise. The at-rest $\dot{V}O_2$ value is taken to be $0.200\ \text{L} \cdot \text{min}^{-1}$. The maximal $\dot{V}O_2$ value is taken to be $1.570\ \text{L} \cdot \text{min}^{-1}$, as observed by Hedlund et al. [19]. The $\dot{V}O_2$ value at moderate exercise is defined to be the average between the at-rest and maximal values corresponding to $0.885\ \text{L} \cdot \text{min}^{-1}$. In analyzing results, we consider the solution at the periodic steady state. Table 1 summarizes the model-predicted hemodynamics for the at-rest, moderate, and maximal exercise scenarios. Fig. 2 displays the pressure-volume relationships and pressure waveforms for these three scenarios. The trends seen in the model predicted variables are consistent with both clinical observations [23] and animal experiments [7], including a decrease in ventricular diastolic pressure and increases in systemic pressures and cardiac output

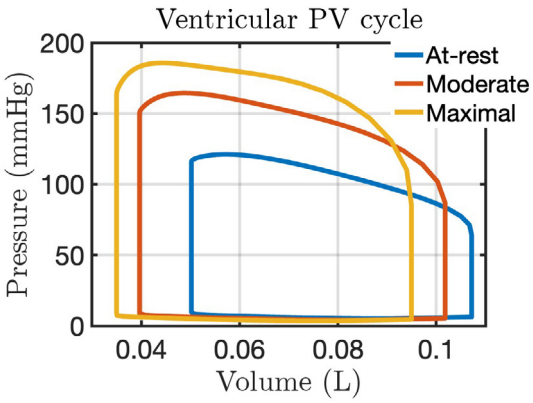

(a) Pressure-volume loop of the ventricle for different exercise intensities.

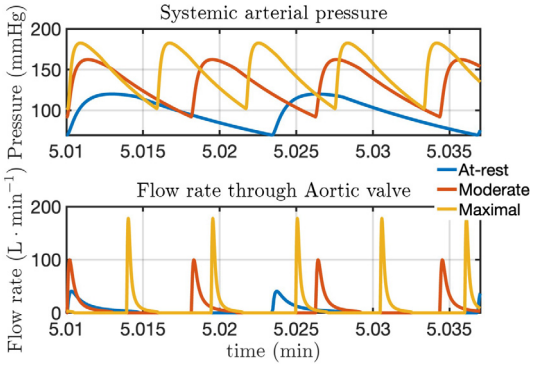

(b) Pressure waveforms in the systemic arteries and flow waveforms through the aortic valve for the different exercise intensities. The figure illustrates two cardiac cycles for the at-rest case as well as the simulated exercise cases for the same period of time.

Fig. 2. Simulation results for the cases of at-rest ($\dot{V}O_2 = 0.200$ L · min^{-1}), moderate exercise ($\dot{V}O_2 = 0.885$ L · min^{-1}), and maximal exercise ($\dot{V}O_2 = 1.570$ L · min^{-1}).

Table 2
Comparison between predicted and measured hemodynamic values. The measurements from Larsson [23] and Shachar [37] were done at $\dot{V}O_2 =$ 1.47 L · min^{-1} and 1.01 L · min^{-1} respectively. A body surface of area of 1.5 m^2 was assumed for the latter study. Simulations are performed using the average oxygen consumption rate between the two studies corresponding to 1.24 L · min^{-1}.

Variable	Numerical	Experiment	Reference
Systolic Blood Pressure (mmHg)	174.55	164	[23]
Diastolic Blood Pressure (mmHg)	98.14	88	[23]
Cardiac Output (L · min^{-1})	9.13	8.0	[23]
Stroke Volume (mL)	61.41	64	[23]
Systemic Oxygen Saturation (%)	95.00	93	[37]
Venous Oxygen Saturation (%)	23.84	31	[37]

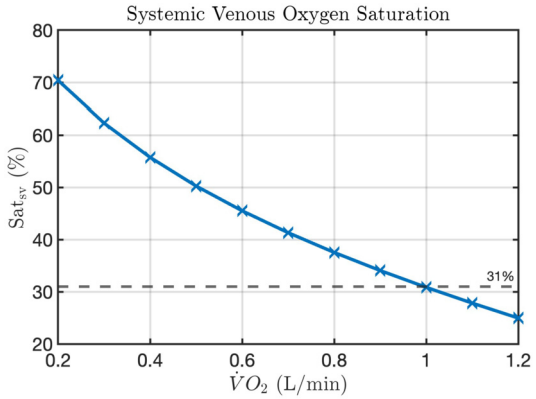

Fig. 3. Systemic venous oxygen concentration (Sat$_{sv}$) as a function of the oxygen consumption rate ($\dot{V}O_2$) for the baseline exercise model. The blue solid line intersects the grey dashed line when the oxygen consumption rate results in a systemic venous concentration of 31%. This value for the consumption is used to estimate $\dot{V}O_2$-max as described in section 2.4.

in exercise. We also note the very mild increase in stroke volume in exercise. This trend seems to align with clinical data from Gewillig et al., who reported that stroke volume did not increase at the same rate as cardiac output, and in their "worst ten" group of Fontan patients, stroke volume decreased with exercise intensity [16].

Next, we compare predictions from our model with the clinical studies of Larsson et al. and Shachar et al. [23,37]. For this comparison, we must determine the value for $\dot{V}O_2$ that is consistent with these studies. Shachar et al. reported a $\dot{V}O_2$ indexed by body surface area of 0.671 L · min^{-1}m^{-2}. With a body surface area of 1.5 m^2, this corresponds to an oxygen consumption rate of 1.01 L · min^{-1}. Larsson et al. reported a $\dot{V}O_2$ of 1.47 L · min^{-1}. For this comparison, we take $\dot{V}O_2$ to 1.24 L · min^{-1} in our model, which is the average of the oxygen consumption rates observed in these two studies. Table 2 shows the values of the model-predicted variables compared against the corresponding clinical data. Our results agree well with the data reported in the two clinical studies.

The exercise tolerance estimation method in section 2.4 requires computing the $\dot{V}O_2$ corresponding to Sat$_{sv} = 31\%$. Since $\dot{V}O_2$ is an independent variable in our model, we achieve this by varying $\dot{V}O_2$ in the range $[0.2, 1.2]$ L · min^{-1} at intervals of 0.1 L · min^{-1} and computing the corresponding Sat$_{sv}$. The functional relationship between Sat$_{sv}$ and $\dot{V}O_2$ predicted from our model is shown in Fig. 3 and called the saturation-consumption curve. The systemic venous oxygen saturation decreases as $\dot{V}O_2$ increases, and we interpolate the points defining this curve to approximate the $\dot{V}O_2$ value that corresponds to Sat$_{sv} = 31\%$. For the baseline exercise model, we obtain $\dot{V}O_2$-max = 1.33 L · min^{-1}, which is close to clinical measurements of $\dot{V}O_2$-max = 1.47 and 1.5 L · min^{-1} [23,26].

3.2. *Effect of systemic arterial compliance on exercise tolerance*

During the first procedure for single ventricle patients with certain physiologies, e.g. hypoplastic left heart syndrome, the surgeon is tasked with reconstructing the aorta and attaching it to the functioning ventricle [32]. This operation tends to decrease the compliance of the aorta [6]. In turn, aortic reconstruction has a significant impact on the downstream compliance felt by the single ventricle over the lifespan of the patient. The combined aortic and downstream vascular compliance is specified in our model by the systemic arterial compliance parameter, denoted C_{sa}. It should be noted that the compliance of the aorta likely accounts for a substantial fraction of the total arterial compliance. For example, in a popular model for the systemic arterial circulation, the aortic compliance accounts for 30-45% of the total compliance, depending on the inclusion of the thoracic aorta into this calculation [39]. We vary the at-rest value, denoted $C_{sa,0}$, in our simulations to study its effect on hemodynamics at rest and in exercise. The parameter C_{sa} in our model is then calculated as a function of the heart rate via equation (9). The saturation-consumption curve is constructed for each value of the systemic arterial compliance. In the baseline model, we take the at-rest value of $C_{sa,0}$ to be 7.33×10^{-4} L · mmHg^{-1}. Then, we run simulations with $C_{sa,0}$ values in the range $[0.91625, 14.66] \times 10^{-4}$ L · mmHg^{-1}. The saturation-consumption curves are constructed as done in section 3.1 and are shown in Fig. 4a. The $\dot{V}O_2$-max values are shown in Fig. 4b. In

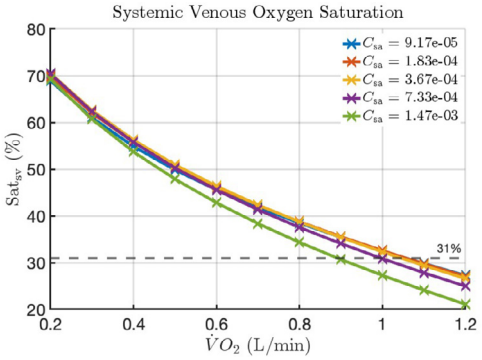

(a) The solid lines show the systemic venous oxygen saturation as a function of the oxygen consumption rate for different values of the systemic arterial compliance C_{sa}. The dashed line at $Sat_{sv} = 31\%$ intersects the solid lines at consumption rates corresponding to 75% of the $\dot{V}O_2$-max.

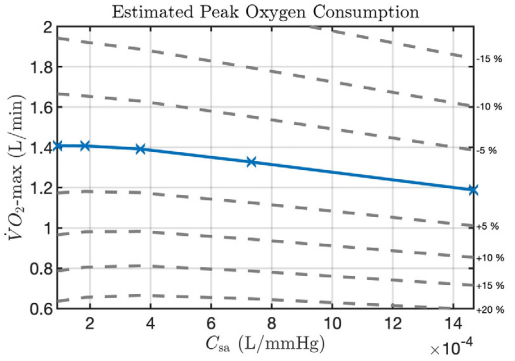

(b) Predicted peak oxygen consumption rates ($\dot{V}O_2$-max) for different values of the systemic arterial compliance C_{sa}. The grey dashed lines indicate the sensitivity of the predicted $\dot{V}O_2$-max to changes in the Sat_{sv} threshold, i.e. the upper and lower lines correspond to Sat_{sv} less than and greater than 31% respectively.

Fig. 4. Effect of the systemic arterial compliance C_{sa} on exercise tolerance.

addition to computing $\dot{V}O_2$-max corresponding to $Sat_{sv} = 31\%$, as discussed in section 2.4, we consider a range of saturation values greater and less than 31% to visualize how the predicted $\dot{V}O_2$-max depends on the choice of threshold saturation value. These results are plotted as grey dashed lines in Fig. 4b.

The model predicts that a very compliant systemic arterial compartment results in a marginally lower exercise tolerance. Further, a stiffer systemic arterial compartment provides only a mild increase in $\dot{V}O_2$-max, if at all. In fact, for the lower dashed lines corresponding to $\dot{V}O_2$-max predicted from $Sat_{sv} > 31\%$, there are decreases in $\dot{V}O_2$-max for smaller compliance values, indicating the curve is non-monotone. In other words, for these cases, the exercise tolerance decreases as the systemic arterial compartment becomes stiffer. This trend has been noted experimentally. Harteveld et al. measured the aortic pulse wave velocity, an indicator of vessel stiffness, and observed a decrease in $\dot{V}O_2$-max as the aortic stiffness increased [18,25]. The apparent detrimental effect of arterial stiffness on exercise tolerance has led some to suggest investigation of aortic reconstruction design, such as the choice of materials that could lead to a more compliant aorta [3]. Our results somewhat corroborate this suggestion; although, as seen in Fig. 4b, the reduction in exercise tolerance is not linear as the increase in exercise tolerance plateaus at low values of the systemic arterial compliance.

3.3. Effect of the total cavopulmonary connection on exercise tolerance

The Fontan circulation is established by a surgical connection between the vena cavae and main pulmonary arteries [10,9]. This connection, called the total cavopulmonary connection (TCPC), allows for passive flow of deoxygenated blood from the systemic veins directly to the lungs. The geometry of the TCPC has a significant effect on the fluid mechanics of the blood entering the lungs. There has been intense research devoted to TCPC design and its impact on flow through the pulmonary arteries. Furthermore, flow resistance due to the TCPC geometry has been observed to affect exercise tolerance [42]. Recent clinical evidence for this includes the analysis of TCPC hemodynamics using 4D flow cardiovascular magnetic resonance imaging [36]. We use our model to systematically investigate the effect of the TCPC design on exercise tolerance. The TCPC geometry is described by the resistance parameter R_{TCPC}, which represents the fluid-mechanical resistance of this surgical connection. We vary R_{TCPC} and construct the corresponding saturation-consumption curves. In the baseline model, R_{TCPC} is set to 10^{-1} mmHg $\cdot$ min $\cdot$ L^{-1}. We consider a range of R_{TCPC} values from 0.25×10^{-1} mmHg $\cdot$ min $\cdot$ L^{-1} to 4×10^{-1} mmHg $\cdot$ min $\cdot$ L^{-1}, which is comparable to values seen in the literature [41,35,44]. The saturation-consumption curves are constructed as done in section 3.1 and are shown in Fig. 5a. The corresponding $\dot{V}O_2$-max values are shown in Fig. 5b.

As seen in Fig. 5b, the model predicts worse exercise tolerance for large R_{TCPC} values. These results suggest that reducing the resistance of the TCPC connection is beneficial. Since the parameter R_{TCPC} describes the geometry dependent resistance of the surgical connection, our results are consistent with prior research that seeks to construct optimal TCPC geometries that minimize flow impedance and energy loss [42].

3.4. Effect of fenestration size on exercise tolerance

Data on the effects of a fenestration on exercise tolerance are inconclusive. Meadows et al. investigated $\dot{V}O_2$-max in Fontan patients with a fenestration and again half a year after they had their fenestration closed. Although a small drop in $\dot{V}O_2$-max was detected, it was not significant. Loomba et al. investigated exercise tolerance in Fontan patients with and without a fenestration [26]. Although the fenestrated group had a lower $\dot{V}O_2$-max, the authors found no significant differences when considering $\dot{V}O_2$-max normalized by body mass [26]. In our framework, the fenestration is described by the nonlinear resistance parameter R_{fen}, which is calculated from equation (3). We investigate the effects of the fenestration by considering the case of no fenestration as well as a range of values for R_{fen}. Although R_{fen} is a function of the fenestration cross-sectional area A_{fen}, for clarity we visualize results as a function of the fenestration diameter d_{fen}. Simulations are run for fenestration diameters varying from 2 mm to 10 mm, and we also include the closed fenestration case corresponding to $d_{fen} = 0$ mm. Saturation-consumption curves are shown in Fig. 6a and the corresponding $\dot{V}O_2$-max values are shown in Fig. 6b.

Fig. 6b demonstrates that the presence of a fenestration decreases $\dot{V}O_2$-max. However, the decrease in exercise tolerance relative to a closed fenestration is not very significant for small fenestration diameters. Meadows et al. noted they initially expected depressed exercise tolerance in the fenestrated case, however, they did not detect any statistically significant changes and postulated that factors such as sample size could have contributed to their insignificant results [29]. When considering the diameter range suggested by Bridges et al. [5] of $4 - 6$ mm, we observe a reduction in $\dot{V}O_2$-max relative to an unfenestrated case of $6.8 - 17.1\%$. In comparison, Meadows et al. reported a 4.4% increase in $\dot{V}O_2$-max after fenestration occlusion. Furthermore, our model predicts that increasing the fenestration diameter beyond

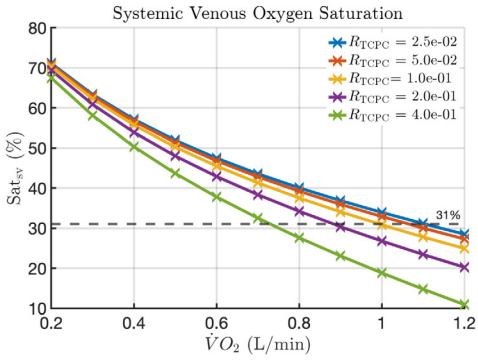

(a) The solid lines show the systemic venous oxygen saturation as a function of the oxygen consumption rate for different values of the total cavopulmonary connection resistance R_{TCPC}. The dashed line at $\mathrm{Sat_{sv}} = 31\%$ intersects the solid lines at consumption rates corresponding to 75% of the $\dot{V}O_2$-max.

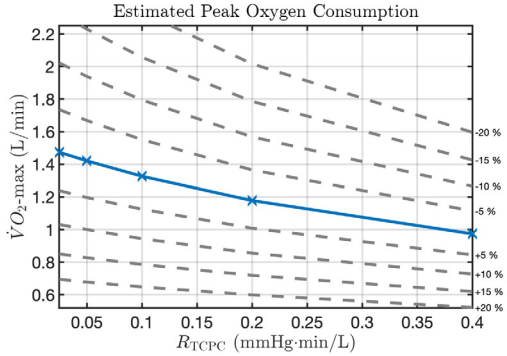

(b) Predicted peak oxygen consumption rates ($\dot{V}O_2$-max) for different values of the total cavopulmonary connection resistance R_{TCPC}. The grey dashed lines indicate the sensitivity of the predicted $\dot{V}O_2$-max to changes in the $\mathrm{Sat_{sv}}$ threshold, i.e. the upper and lower lines correspond to $\mathrm{Sat_{sv}}$ less than and greater than 31% respectively.

Fig. 5. Effect of the total cavopulmonary connection resistance R_{TCPC} on exercise tolerance.

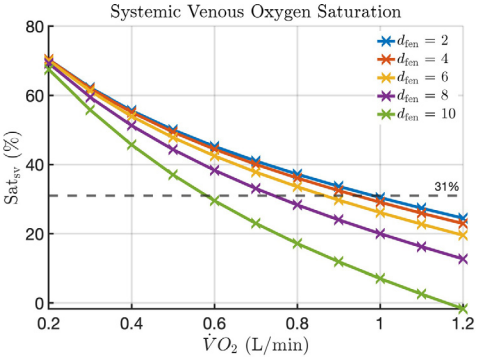

(a) The solid lines show the systemic venous oxygen saturation as a function of the oxygen consumption rate for different values of the fenestration diameter d_{fen}. The dashed line at $\mathrm{Sat_{sv}} = 31\%$ intersects the solid lines at consumption rates corresponding to 75% of the $\dot{V}O_2$-max.

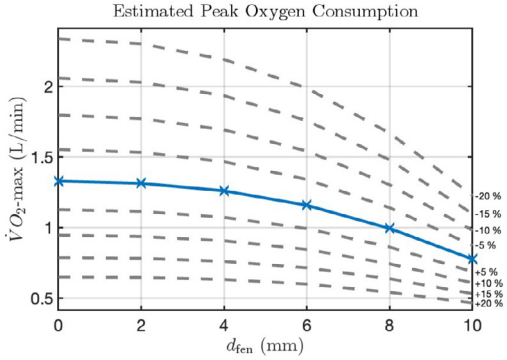

(b) Predicted peak oxygen consumption rates ($\dot{V}O_2$-max) for different values of the fenestration diameter d_{fen}. The grey dashed lines indicate the sensitivity of the predicted $\dot{V}O_2$-max to changes in the $\mathrm{Sat_{sv}}$ threshold, i.e. the upper and lower lines correspond to $\mathrm{Sat_{sv}}$ less than and greater than 31% respectively.

Fig. 6. Effect of the fenestration size on exercise tolerance.

this range of values contributes to a more significant impairment of exercise tolerance, since Fig. 6b indicates a negative second derivative of $\dot{V}O_2$-max with respect to the fenestration diameter.

3.5. Sensitivity analysis

In this section, we quantify the relative sensitivities of $\dot{V}O_2$-max with respect to several of the model parameters, including the power law exponents in the exercise model. The relative sensitivity of $\dot{V}O_2$-max with respect to a parameter X, evaluated at a nominal value X_0, is defined as:

$$\frac{X_0}{\dot{V}O_2\text{-max}(X_0)} \left.\frac{\partial \dot{V}O_2\text{-max}(X)}{\partial X}\right|_{X_0}. \tag{13}$$

The partial derivative in equation (13) is approximated with a centered finite difference:

$$\left.\frac{\partial \dot{V}O_2\text{-max}(X)}{\partial X}\right|_{X_0} \approx \frac{\dot{V}O_2\text{-max}(X_{0,\mathrm{up}}) - \dot{V}O_2\text{-max}(X_{0,\mathrm{low}})}{X_{0,\mathrm{up}} - X_{0,\mathrm{low}}}. \tag{14}$$

The values $X_{0,\mathrm{up}}, X_{0,\mathrm{low}}$ are upper and lower bounds around the nominal value X_0. For our analysis, we take $X_{0,\mathrm{up}} = 1.1\ X_0$ and $X_{0,\mathrm{low}} = 0.9\ X_0$.

First, sensitivities are computed with respect to the three surgically determined parameters that are the focus of this paper: the arterial compliance C_{sa}, the resistance of the total cavopulmonary connection R_{TCPC}, and the fenestration diameter d_{fen}. Sensitivities for the systemic arterial compliance and the TCPC resistance are evaluated at the values used in the baseline exercise model, discussed in section 2.3. The sensitivity for the fenestration diameter is evaluated at sizes bounded away from zero: $d_{\mathrm{fen}} = 4$ mm and 8 mm. Sensitivity results are shown in Table 3. $\dot{V}O_2$-max appears to be least sensitive to C_{sa}, but the sensitivities for R_{TCPC} and the 4 mm fenestration are similar. The larger 8 mm fenestration has a sensitivity five times as large as the smaller fenestration, which seems to be consistent with the variation of $\dot{V}O_2$-max with respect to fenestration size as seen in Fig. 6b.

Given the uncertainty and variability in the empirical data that was used to calibrate the exercise model, as described in section 2.3, we calculate sensitivities of $\dot{V}O2$-max with respect to the power law exponents that determine this model. Table 4 contains these sensitivities,

Table 3
Sensitivities of $\dot{V}O_2$-max to the surgically determined parameters.

Variable	Sensitivity
R_{TCPC}	-11.97%
C_{sa}	-9.73%
$d_{\text{fen}} = 4$ mm	-10.60%
$d_{\text{fen}} = 8$ mm	-54.45%

Table 4
Sensitivities of $\dot{V}O_2$-max to the power law exponent γ in the exercise model.

Exponent γ for Variable	Sensitivity
C_{sa}	2.02%
R_{s}	7.40%
$V_{\text{d,sv}}$	22.17%
C_{sys}	14.38%
C_{dias}	9.05%

which in general are relatively small. The exponent for the dead volume in the systemic veins has the largest sensitivity. This result seems consistent with the notion that hemodynamics are generally sensitive to changes in blood volume, and variations in the exponent for $V_{\text{d,sv}}$ affect mobilization of additional blood volume in exercise.

4. Conclusions

In this paper, we constructed a model for the Fontan circulation that includes a fenestration. The model predicts pressures, flows, and oxygen concentrations in the major compartments of the circulation. An approach for describing exercise within this framework was presented, which modulates parameters as functions of the exercise intensity, determined by the systemic oxygen consumption. We derived a heuristic, based on clinical data from Fontan patients, for estimating $\dot{V}O_2$-max from the model predicted variables. $\dot{V}O_2$-max was then used to study Fontan exercise tolerance within this framework.

We first verified that the model was able to reasonably predict Fontan hemodynamics at rest and in exercise, when compared against results of clinical studies. The hemodynamic parameters in the baseline at-rest model were based on experimental data and previously reported values [1,41]. Independently, the power law exponents for C_{sa}, R_{s}, and C_{sys} in the exercise model were determined from empirical data. We were unable to find data in order to approximate the power law exponent for the dead volume $V_{\text{d,sv}}$, so this was based on the value used by Han et al. [17]. Finally, the power law exponent for C_{dias} was calibrated based on clinical estimates of $\dot{V}O_2$-max [23,26].

The framework was then applied to study the effect of surgical interventions on exercise tolerance, as quantified by the model predicted $\dot{V}O_2$-max. We found that larger systemic arterial compliance values tend to decrease exercise tolerance, which extends the current clinical understanding that a more compliant reconstructed aorta may not always be strictly beneficial. The resistance of the TCPC junction was found to negatively impact exercise tolerance. This corroborates efforts to use high-fidelity models to compute optimal TCPC geometries that minimize energy loss. Lastly, an increasing fenestration size was found to decrease exercise tolerance. However, for a range of typical fenestration sizes, this drop was relatively small, which may explain why it is challenging to observe significant differences in exercise tolerance between fenestrated and unfenestrated patients. Sensitivity analysis suggested that exercise tolerance is similarly sensitive to the resistance of the total cavopulmonary connection, small fenestrations, and the systemic arterial compliance. Sensitivity of exercise tolerance to a larger fenestration was substantially higher than the sensitivities to the other parameters.

Declaration of competing interest

None.

Acknowledgements

BR acknowledges partial support from NSF-DMS 2111459 and 1913291.

Appendix A

A.1. Governing equations

The volume of compartment i is defined to be the sum of the dead volume $V_{d,i}$ and the product of the compliance C_i and the pressure P_i:

$$V_i = V_{d,i} + C_i P_i.$$

Conservation of volume in each compartment leads to a system of nonlinear ODEs for the pressures:

$$\frac{d(C_{\text{vc}}P_{\text{vc}})}{dt} = S_{\text{pv,vc}}\frac{1}{R_{\text{av}}}(P_{\text{pv}} - P_{\text{vc}}) - S_{\text{vc,sa}}\frac{1}{R_{\text{ao}}}(P_{\text{vc}} - P_{\text{sa}})$$

$$\frac{d(C_{\text{sa}}P_{\text{sa}})}{dt} = S_{\text{vc,sa}}\frac{1}{R_{\text{ao}}}(P_{\text{vc}} - P_{\text{sa}}) - \frac{1}{R_{\text{s}}}(P_{\text{sa}} - P_{\text{sv}})$$

$$\frac{d(C_{\text{sv}}P_{\text{sv}})}{dt} = \frac{1}{R_{\text{s}}}(P_{\text{sa}} - P_{\text{sv}}) - \frac{1}{R_{\text{TCPC}}}(P_{\text{sv}} - P_{\text{pa}}) - \frac{\delta_{\text{fen}}}{R_{\text{fen}}}(P_{\text{sv}} - P_{\text{pv}})$$

$$\frac{d(C_{\text{pa}}P_{\text{pa}})}{dt} = \frac{1}{R_{\text{TCPC}}}(P_{\text{sv}} - P_{\text{pa}}) - \frac{1}{R_{\text{p}}}(P_{\text{pa}} - P_{\text{pv}})$$

$$\frac{d(C_{\text{pv}}P_{\text{pv}})}{dt} = \frac{1}{R_{\text{p}}}(P_{\text{pa}} - P_{\text{pv}}) + \frac{\delta_{\text{fen}}}{R_{\text{fen}}}(P_{\text{sv}} - P_{\text{pv}}) - S_{\text{pv,vc}}\frac{1}{R_{\text{av}}}(P_{\text{pv}} - P_{\text{vc}}).$$

The subscripts label the compliance chambers in the model, i.e. vc = ventricular chamber, sa = systemic arteries, sv = systemic veins, pa = pulmonary arteries, pv = pulmonary veins, TCPC = total cavopulmonary connection, and fen = fenestration. The parameter δ_{fen} is set to 1 when the fenestration is open and 0 when the fenestration is closed. Recall that R_{fen} is a function of the term $|P_{\text{sv}} - P_{\text{pv}}|$. The term S_{ij} represents the path's flow state. This term can be written in terms of the pressure as $S_{ij} = \text{logical}(P_i > P_j)$, i.e. S_{ij} is set to 1 if $P_i > P_j$ and to 0 otherwise. The term S_{ij} is used to describe the valves upstream and downstream from the ventricular chamber compartment. For the other paths, flow in both directions is allowed in the model.

Conservation of oxygen volume in each compartment leads to the following system of ODEs:

$$\frac{d}{dt}(V_{\text{vc}}\,\sigma_{\text{vc}}) = S_{\text{pv,vc}}\frac{1}{R_{\text{av}}}(P_{\text{pv}} - P_{\text{vc}})\sigma_{\text{pv}} - S_{\text{vc,sa}}\frac{1}{R_{\text{ao}}}(P_{\text{vc}} - P_{\text{sa}})\sigma_{\text{vc}}$$

$$\frac{d}{dt}(V_{\text{sa}}\,\sigma_{\text{sa}}) = S_{\text{vc,sa}}\frac{1}{R_{\text{ao}}}(P_{\text{vc}} - P_{\text{sa}})\,\sigma_{\text{vc}} - \frac{1}{R_{\text{s}}}(P_{\text{sa}} - P_{\text{sv}})\left(S_{\text{sa,sv}}\sigma_{\text{sa}} + S_{\text{sv,sa}}\sigma_{\text{sv}}\right)$$

$$\frac{d}{dt}(V_{\text{sv}}\,\sigma_{\text{sv}}) = \frac{1}{R_{\text{s}}}(P_{\text{sa}} - P_{\text{sv}})\left(S_{\text{sa,sv}}\sigma_{\text{sa}} + S_{\text{sv,sa}}\sigma_{\text{sa}}\right) - \frac{1}{R_{\text{TCPC}}}(P_{\text{sv}} - P_{\text{pa}})\left(S_{\text{sv,pa}}\sigma_{\text{sv}} + S_{\text{pa,sv}}\sigma_{\text{pa}}\right) - \frac{\delta_{\text{fen}}}{R_{\text{fen}}}(P_{\text{sv}} - P_{\text{pv}})\left(S_{\text{sv,pv}}\sigma_{\text{sv}} + S_{\text{pv,sv}}\sigma_{\text{pv}}\right) - \dot{V}O_2$$

$$\frac{d}{dt}(V_{\text{pa}}\,\sigma_{\text{pa}}) = \frac{1}{R_{\text{TCPC}}}(P_{\text{sv}} - P_{\text{pa}})\left(S_{\text{sv,pa}}\sigma_{\text{sv}} + S_{\text{pa,sv}}\sigma_{\text{pa}}\right) - \frac{1}{R_{\text{p}}}(P_{\text{pa}} - P_{\text{pv}})\left(S_{\text{pa,pv}}\sigma_{\text{pa}} + S_{\text{pv,pa}}\sigma_{\text{pv}}\right)$$

$$\frac{d}{dt}(V_{\text{pv}}\,\sigma_{\text{pv}}) = \frac{1}{R_{\text{p}}}(P_{\text{pa}} - P_{\text{pv}})(S_{\text{pa,pv}}\overline{\sigma} + S_{\text{pv,pa}}\sigma_{\text{pv}})$$

$$- S_{\text{pv,vc}} \frac{1}{R_{\text{av}}} (P_{\text{pv}} - P_{\text{vc}}) \sigma_{\text{pv}}$$
$$+ \frac{\delta_{\text{fen}}}{R_{\text{fen}}} (P_{\text{sv}} - P_{\text{pv}}) \left(S_{\text{sv,pv}} \sigma_{\text{sv}} + S_{\text{pv,sv}} \sigma_{\text{pv}} \right)$$

The source term $\overline{\sigma}$ is the volumetric concentration corresponding to full saturation, assumed to be $\text{Sat}_{\text{pv}} = 95\%$ [26]. Note that the sink term $-\dot{V}O_2$ assumes the systemic venous compartment is in steady-state with the tissues. As a result, the oxygen uptake in the bloodstream is equal to the oxygen consumption of the tissues.

A.2. Parameters

Parameters needed for the time-dependent ventricular compliance as well as the additional compliance values are:

$$C_{\text{dias},0} = 1/79.52 \text{ L} \cdot \text{mmHg}^{-1}, \quad C_{\text{sys},0} = 1/5232 \text{ L} \cdot \text{mmHg}^{-1},$$
$$\tau_1 = 0.269\, T, \quad \tau_2 = 0.452\, T, \quad m_1 = 1.32, \quad m_2 = 27.4$$
$$C_{\text{sv}} = 0.099 \text{ L} \cdot \text{mmHg}^{-1}, \quad C_{\text{pa}} = 0.00412 \text{ L} \cdot \text{mmHg}^{-1},$$
$$C_{\text{pv}} = 0.01 \text{ L} \cdot \text{mmHg}^{-1} \quad C_{\text{sa},0} = 0.000733 \text{ L} \cdot \text{mmHg}^{-1}$$

The compliances C_{sa}, C_{sys}, and C_{dias} are determined from (9), (11), and (12) respectively. Resistance values are:

$$R_{\text{av}} = 0.01 \text{ mmHg} \cdot \text{min} \cdot \text{L}^{-1}, \quad R_{\text{ao}} = 0.2 \text{ mmHg} \cdot \text{min} \cdot \text{L}^{-1},$$
$$R_{\text{TCPC}} = 0.1 \text{ mmHg} \cdot \text{min} \cdot \text{L}^{-1}, \quad R_{\text{p}} = 0.5517 \text{ mmHg} \cdot \text{min} \cdot \text{L}^{-1},$$
$$R_{\text{s},0} = 20.78 \text{ mmHg} \cdot \text{min} \cdot \text{L}^{-1}.$$

Note that R_{fen} is calculated as a nonlinear function of the pressures and depends on the viscous resistance, density, and fenestration size. The resistance R_{s} is determined by (8). The compartment dead volumes are:

$$V_{d,\text{vc}} = 0.028 \text{ L}, \quad V_{d,\text{sa}} = 0.7051 \text{ L}, \quad V_{d,\text{pa}} = 0.093 \text{ L},$$
$$V_{d,\text{pv}} = 0.1475 \text{ L}, \quad V_{d,\text{sv},0} = 2.869 \text{ L}.$$

Note that $V_{d,\text{sv}}$ is given by (10). Finally, the parameter

$$\overline{\sigma} = 0.191,$$

to ensure that the blood in the pulmonary veins corresponds to a saturation of 95%.

A.3. Discretized system and algorithm

We apply the model to the network representing the Fontan physiology in Fig. 1. Furthermore, we discretize the differential equations with the backward Euler method using timestep $\tau > 0$. Let the subscripts refer to the compartment and the superscripts refer to the time at which the variable state is evaluated. $\mathbf{V}, \mathbf{P}, \sigma, \mathbf{C}$, and $\mathbf{R}$ refer to the compartmental volume, pressure, volumetric concentration, compliance, and resistance in vector form, respectively. The matrix $\mathbf{S}$ denotes the flow state between compartments. The matrix $\mathbf{U}$ denotes oxygen volume per unit time flowing between compartments. The backward Euler discretization results in the system,

$$\underbrace{\begin{bmatrix} \mathbf{A}_1 & \underline{0} \\ \underline{0} & \mathbf{A}_2 \end{bmatrix}}_{\Lambda} \underbrace{\begin{bmatrix} \mathbf{P} \\ \boldsymbol{\sigma} \end{bmatrix}^t}_{y} = \underbrace{\begin{bmatrix} \mathbf{b}_1 \\ \mathbf{b}_2 \end{bmatrix}}_{\zeta}, \tag{15}$$

where:

$$\mathbf{A}_1 = \text{diag}(\mathbf{C}^t - (\text{sum}(\mathbf{E}))^T) + \mathbf{E},$$
$$\mathbf{b}_1 = \mathbf{C}^{t-\Delta t} \odot \mathbf{P}^{t-\Delta t},$$
$$\mathbf{A}_2 = \Delta t\, (\mathbf{S}^t \odot \mathbf{G})^T \odot \mathbf{\Delta P}^t + \text{diag}(\mathbf{V}^t) + \Delta t\, \text{diag}((\mathbf{S}^t \odot \mathbf{G} \odot \mathbf{\Delta P}^t)\vec{1}),$$
$$\mathbf{b}_2 = \mathbf{V}^{t-\Delta t} \odot \sigma^{t-\Delta t} + \Delta t\, ((\mathbf{U}^t \odot \mathbf{S}^t)^T \vec{1}).$$

The following abbreviations and notations were used:

$$\mathbf{G} = 1/\mathbf{R},$$
$$\mathbf{E} = \Delta t((\mathbf{S}^t \odot \mathbf{G}) + (\mathbf{S}^t \odot \mathbf{G})^T),$$
$$\Delta P_{i,j} = P_i - P_j,$$
$$\vec{1} : = \text{one vector},$$
$$\odot : = \text{element-wise multiplication}.$$

Algorithm 1 below details the numerical implementation for the discrete system to compute the state variable $\mathbf{y} = [P_i, \sigma_i]$.

Algorithm 1 Numerical scheme using backward Euler discretization and Picard iterations.

Given the initial vector y_{ini}
Given the number of time steps $klokmax$
Given a tolerance tol
Initialize compartment network
$y \leftarrow y_{ini}$
for $m = 0, 1, ..., klokmax - 1$ **do**
  $\tilde{y} \leftarrow y$
  $\Delta \leftarrow \infty$
  while $\Delta > tol$ **do** ▷ Picard iteration loop
    if network is fenestrated **then**
      $R_{\text{fen}}(\tilde{y}) \leftarrow$ positive root of (3)
    end if
    $\mathbf{S}(\tilde{y}) \leftarrow logical(P < P^T)$
    form $\Lambda(\tilde{y})$, $\zeta(\tilde{y})$ from (15) at current m ▷ Backward Euler discretization
    $\Delta \leftarrow ||\tilde{y} - \Lambda \backslash \zeta||$
    $\tilde{y} \leftarrow \Lambda \backslash \zeta$
  end while
  $y \leftarrow \tilde{y}$
end for
return y

References

[1] Ahmad Zan, Jin Lynn H, Penny Daniel J, Rusin Craig G, Peskin Charles S, Puelz Charles. Optimal fenestration of the Fontan circulation. Front Physiol 2022;13:867995.

[2] Biglino Giovanni, Schievano Silvia, Steeden Jennifer A, Ntsinjana Hopewell, Baker Catriona, Khambadkone Sachin, et al. Reduced ascending aorta distensibility relates to adverse ventricular mechanics in patients with hypoplastic left heart syndrome: noninvasive study using wave intensity analysis. J Thorac Cardiovasc Surg 2012;144(6):1307–14.

[3] Biko David M, Gaynor J William, Partington Sara L, Harris Matthew A, Whitehead Kevin K, Trusty Phillip, et al. Relationship of aortic stiffness to exercise and ventricular volumes in single ventricles. Ann Thorac Surg 2019;108(2):574–80.

[4] Brassard Patrice, Bédard Élisabeth, Jobin Jean, Rodés-Cabau Josep, Poirier Paul. Exercise capacity and impact of exercise training in patients after a Fontan procedure: a review. Can J Cardiol 2006;22(6):489–95.

[5] Bridges Nancy D, Lock James E, Castaneda Aldo R. Baffle fenestration with subsequent transcatheter closure. Modification of the Fontan operation for patients at increased risk. Circulation 1990;82(5):1681–9.

[6] Cardis Brian M, Fyfe Derek A, Mahle William T. Elastic properties of the reconstructed aorta in hypoplastic left heart syndrome. Ann Thorac Surg 2006;81(3):988–91.

[7] Cheng Che-Ping, Igarashi Yuichiro, Little William C. Mechanism of augmented rate of left ventricular filling during exercise. Circ Res 1992;70(1):9–19.

[8] Collins Julie-Ann, Rudenski Aram, Gibson John, Howard Luke, o'Driscoll Ronan. Relating oxygen partial pressure, saturation and content: the haemoglobin–oxygen dissociation curve. Breathe 2015;11(3):194–201.

[9] De Leval Marc R. The Fontan circulation: a challenge to William Harvey? Nat Clin Pract Cardiovasc Med 2005;2(4):202–8.

[10] de Leval Marc R, Kilner Philip, Gewillig Marc, Bull Catherine, McGoon Dwight C. Total cavopulmonary connection: a logical alternative to atriopulmonary connection for complex Fontan operations: experimental studies and early clinical experience. J Thorac Cardiovasc Surg 1988;96(5):682–95.

[11] DeGroff Curt G. Modeling the Fontan circulation: where we are and where we need to go. Pediatr Cardiol 2008;29(1):3–12.

[12] Diller Gerhard-Paul, Dimopoulos Konstantinos, Okonko Darlington, Li Wei, Babu-Narayan Sonya V, Broberg Craig S, et al. Exercise intolerance in adult congenital heart disease: comparative severity, correlates, and prognostic implication. Circulation 2005;112(6):828–35.
[13] Driscoll David J, Offord Kenneth P, Feldt Robert H, Schaff Hartzell V, Puga Francisco J, Danielson Gordon K. Five-to fifteen-year follow-up after Fontan operation. Circulation 1992;85(2):469–96.
[14] Fontan Francis, Baudet Eugene. Surgical repair of tricuspid atresia. Thorax 1971;26(3):240–8.
[15] Gewillig Marc, Brown Stephen C. The Fontan circulation after 45 years: update in physiology. Heart 2016;102(14):1081–6.
[16] Gewillig Marc H, Lundström Ulla R, Bull Catherine, Wyse Richard KH, Deanfield John E. Exercise responses in patients with congenital heart disease after Fontan repair: patterns and determinants of performance. J Am Coll Cardiol 1990;15(6):1424–32.
[17] Han Seong Woo, Puelz Charles, Rusin Craig G, Penny Daniel J, Coleman Ryan, Peskin Charles S. Computer simulation of surgical interventions for the treatment of refractory pulmonary hypertension. Math Med Biol 2022.
[18] Harteveld Lisette M, Blom Nico A, de Los Monteros Covadonga Terol Espinosa, Van Dijk J Gert, Kuipers Irene M, Rammeloo Lukas AJ, et al. Determinants of exercise limitation in contemporary paediatric Fontan patients with an extra cardiac conduit. Int J Cardiol 2021;341:31–8.
[19] Hedlund Eva R, Söderström Liselott, Lundell Bo. Appropriate heart rate during exercise in Fontan patients. Cardiol Young 2020;30(5):674–80.
[20] Hock Julia, Reiner Barbara, Neidenbach Rhoia C, Oberhoffer Renate, Hager Alfred, Ewert Peter, et al. Functional outcome in contemporary children with total cavopulmonary connection–health-related physical fitness, exercise capacity and health-related quality of life. Int J Cardiol 2018;255:50–4.
[21] Kung Ethan, Pennati Giancarlo, Migliavacca Francesco, Hsia Tain-Yen, Figliola Richard, Marsden Alison, et al. A simulation protocol for exercise physiology in Fontan patients using a closed loop lumped-parameter model. J Biomech Eng 2014;136(8).
[22] Kung Ethan, Perry James C, Davis Christopher, Migliavacca Francesco, Pennati Giancarlo, Giardini Alessandro, et al. Computational modeling of pathophysiologic responses to exercise in Fontan patients. Ann Biomed Eng 2015;43:1335–47.
[23] Larsson Eva Strömva, Eriksson Bengt O. Haemodynamic adaptation during exercise in Fontan patients at a long-term follow-up. Scand Cardiovasc J 2003;37(2):107–12.
[24] Larsson Eva Strömvall, Eriksson Bengt O, Sixt Rune. Decreased lung function and exercise capacity in Fontan patients. A long-term follow-up. Scand Cardiovasc J 2003;37(1):58–63.
[25] Laurent Stephane, Cockcroft John, Van Bortel Luc, Boutouyrie Pierre, Giannattasio Cristina, Hayoz Daniel, et al. Expert consensus document on arterial stiffness: methodological issues and clinical applications. Eur Heart J 2006;27(21):2588–605.
[26] Loomba Rohit S, Danduran Michael E, Dixon Jennifer E, Rao Rohit P. Effect of Fontan fenestration on regional venous oxygen saturation during exercise: further insights into Fontan fenestration closure. Pediatr Cardiol 2014;35(3):514–20.
[27] Mahle William T, Rychik Jack, Weinberg Paul M, Cohen Meryl S. Growth characteristics of the aortic arch after the norwood operation. J Am Coll Cardiol 1998;32(7):1951–4.
[28] Marsden Alison L, Vignon-Clementel Irene E, Chan Frandics P, Feinstein Jeffrey A, Taylor Charles A. Effects of exercise and respiration on hemodynamic efficiency in cfd simulations of the total cavopulmonary connection. Ann Biomed Eng 2007;35:250–63.
[29] Meadows Jeffery, Lang Peter, Marx Gerald, Rhodes Jonathan. Fontan fenestration closure has no acute effect on exercise capacity but improves ventilatory response to exercise. J Am Coll Cardiol 2008;52(2):108–13.
[30] Najjar Samer S, Schulman Steven P, Gerstenblith Gary, Fleg Jerome L, Kass David A, O'Connor Frances, et al. Age and gender affect ventricular-vascular coupling during aerobic exercise. J Am Coll Cardiol 2004;44(3):611–7.
[31] Otsuki T, Maeda S, Iemitsu M, Saito Y, Tanimura Y, Ajisaka R, et al. Contribution of systemic arterial compliance and systemic vascular resistance to effective arterial elastance changes during exercise in humans. Acta Physiol 2006;188(1):15–20.
[32] Pigott John D, Murphy John D, Barber Gerald, Norwood William I. Palliative reconstructive surgery for hypoplastic left heart syndrome. Ann Thorac Surg 1988;45(2):122–8.
[33] Pittman Roland N. Regulation of tissue oxygenation. Colloquium series on integrated systems physiology: from molecule to function to disease, vol. 8. Morgan & Claypool Life Sciences; 2016. i-99.
[34] Rijnberg Friso M, Hazekamp Mark G, Wentzel Jolanda J, De Koning Patrick JH, Westenberg Jos JM, Jongbloed Monique RM, et al. Energetics of blood flow in cardiovascular disease: concept and clinical implications of adverse energetics in patients with a Fontan circulation. Circulation 2018;137(22):2393–407.
[35] Rijnberg Friso M, van 't Hul Luca C, Hazekamp Mark G, van den Boogaard Pieter J, Juffermans Joe F, Lamb Hildo J, et al. Haemodynamic performance of 16–20-mm extracardiac Goretex conduits in adolescent Fontan patients at rest and during simulated exercise. Eur J Cardio-Thoracic Surg 2022;63(1):ezac522.
[36] Rijnberg Friso M, Westenberg Jos JM, van Assen Hans C, Juffermans Joe F, Kroft Lucia JM, van den Boogaard Pieter J, et al. 4D flow cardiovascular magnetic resonance derived energetics in the Fontan circulation correlate with exercise capacity and CMR-derived liver fibrosis/congestion. J Cardiovasc Magn Reson 2022;24(21).
[37] Shachar Giora B, Fuhrman Bradley P, Wang Yang, Jr Russell V Lucas, Lock James E. Rest and exercise hemodynamics after the Fontan procedure. Circulation 1982;65(6):1043–8.
[38] Shephard Roy J, Allen C, Benade AJS, Davies CTM, Di Prampero PE, Hedman R, et al. The maximum oxygen intake: an international reference standard of cardiorespiratory fitness. Bull World Health Organ 1968;38(5):757.
[39] Stergiopulos N, Young DF, Rogge TR. Computer simulation of arterial flow with applications to arterial and aortic stenoses. J Biomech 1992;25(12):1477–88.
[40] Sunagawa Hiroshi, Honda Sunao, Mizoguchi Yasuhiro, Yoshii Kaoru, Iwao Hatsuo. Physiological significance of the slope of the regression equation between oxygen consumption and heart rate in exercise testing: the 8th conference on prevention for rheumatic fever and rheumatic heart disease. Jpn Circ J 1984;48(12):1399–401.
[41] Sundareswaran Kartik S, Pekkan Kerem, Dasi Lakshmi P, Whitehead Kevin, Sharma Shiva, Kanter Kirk R, et al. The total cavopulmonary connection resistance: a significant impact on single ventricle hemodynamics at rest and exercise. Am J Physiol, Heart Circ Physiol 2008;295(6):H2427–35.
[42] Tang Elaine, Wei Zhenglun Alan, Whitehead Kevin K, Khiabani Reza H, Restrepo Maria, Mirabella Lucia, et al. Effect of Fontan geometry on exercise haemodynamics and its potential implications. Heart 2017;103(22):1806–12.
[43] Udholm Sebastian, Aldweib Nael, Hjortdal Vibeke Elisabeth, Veldtman Gruschen R. Prognostic power of cardiopulmonary exercise testing in Fontan patients: a systematic review. Open Heart 2018;5(1):e000812.
[44] Whitehead Kevin K, Pekkan Kerem, Kitajima Hiroumi D, Paridon Stephen M, Yoganathan Ajit P, Fogel Mark A. Nonlinear power loss during exercise in single-ventricle patients after the Fontan: insights from computational fluid dynamics. Circulation 2007;116(11_supplement). I–165.